Nanoarchitecture CD@CMC@$MnSiO_3$: A dual responsive drug delivery system with cellular imaging ability

PRABHA BHARTIYA AND P.K. DUTTA*

Polymer Research Laboratory, Department of Chemistry,
Motilal Nehru National Institute of Technology,
Allahabad-211004, India

ABSTRACT

Designing theranostic agents that are responsive to mildly acidic and reducing tumor microenvironments for optimized imaging and chemotherapeutic effects, is of huge interest in nanomedicine. In this context, we have prepared mesoporous manganese silicate NPs and a biocompatible coating of carboxymethyl chitosan (CMC) was introduced on the surface of manganese silicate nanoparticles. In order to confer multifunctionality to the prepared nanovehicle, it was treated hydrothermally which resulted in formation of fluorescent C-dots on the surface of nanovehicle. The nanoarchitecture CD@CMC@$MnSiO_3$ was characterized by FTIR, XRD, UV-visible and PL spectroscopy. A hydrophobic drug curcumin was loaded on the prepared nanoarchitecture and very high drug loading capacity was obtained. Drug release profile was observed at physiological pH (pH 7.4), acidic pH (pH 6.4 and 5.0) and acidic pH with reducing environment (pH 5.0 and glutathione). The prepared nanoarchitecture demonstrated exceptional pH-modulated drug release which was further enhanced in the presence of glutathione. Cellular imaging experiments conducted on SW480 cell lines confirmed potential applicability of the prepared nanoarchitecture for live cellular imaging which may also be applied for tracking of drug.

KEYWORDS: *Carboxymethyl chitosan, Manganese silicate, Glutathione, Drug release, Cellular imaging*

J. Polym. Mater. Vol. **35,** No. 1, 2018, 85-101

Correspondence author e-mail: pkd@mnnit.ac.in

INTRODUCTION

Intriguing fascinating properties of nanomaterials have attracted the researchers in the field of biomedical application especially in oncology because nanomaterials have the ability to be accumulated in leaky vasculatures of tumours due to the so called enhanced permeation and retention effect. Nanomaterials based multifunctional theranostics is a fast exploring field since last one or two decades and it has opened new avenues for precise therapy and diagnosis of cancer[1-4]. Nanomaterial based drug delivery systems can be categorized as: organic, inorganic and hybrid organic-inorganic nanovehicles[5,6]. Fascinating properties of inorganic nanoparticles (NPs) i.e. stability in physiological conditions, ease of functionalization and many other physiochemical properties have enormously attracted scientific community worldwide. But their clinical translation is still a challenge due to limited available data proving their bio-safety especially in terms of low bio-degradation[7]. As one of the representatives of inorganic nanocarriers, mesoporous silica NPs[8,9] have gained enormous attention and are extensively used for biosensing[10], molecular imaging[11], drug delivery[12-15], and syneristic cancer therapy[16-18]. However, biodegradability of silica NPs is still a critical issue due to physiologically inert nature of -Si-O-Si- framework. The reluctant biodegradability of mesoporous silica NPs may lead to the accumulation of the carriers within the body, raising concern for potential bio-safety.

Another desired property of an ideal drug delivery vehicle is bio-responsive function sensitivity for different intracellular signals- low pH, temperature, enzyme and redox potential, which may be helpful in overcoming the issue of low specificity in tumor area[19-21]. This remarkable advantage of tumor microenvironment responsive drug delivery vehicle is very useful in enhancement of chemotherapeutic efficacy and reducing side-effects on normal tissues[22,23]. To promote the biodegradability of silica NPs is still a challenging area of research. Recently, Yu et al. carried out an interesting work to regulate the biodegradation of silica framework by metal-ion doping approach[24]. The biodegradation of silica framework was promoted by disintegration of Mn-O bonds in tumor mimicking acidic and reducing environment of glutathione, which further accelerated biodegradation of silica framework. Choosing manganese ions for metal ion-doping in silica framework is also on safer side in conjugation with bio-safety as it is one of the necessary element in our body for metabolism and it can easily regulate its uptake and excretion [25]. Several reports have also delineated that *in situ* metal silicate growth on silica NPs by self-sacrifice of silica layers results in formation of hierarchical mesoporous silicate shell[26-29]. However, strong alkaline medium was employed in above reported *in situ* silicate methods.

In order to render water dispersibility and extend blood circulation for efficient tumor accumulation and surface modification, different polymers such as chitosan, PEG, PVP, poly(acrylic acid) are usually used[30-34]. Chitosan, second most abundant natural biopolymer composed of D-glucosamine and *N*-acetyl glucosamine units have been extensively used in drug delivery, gene delivery, tissue engineering, wound healing and other biomedical application owing to its

biocompatibility, biodegradability, hemostatic, antibacterial, anti-fungal cationic nature to enhance cellular binding, and low-cost[35-39]. However, application of chitosan is limited by its poor solubility in neutral or basic pH range. Carboxymethyl chitosan (CMC), a kind of chitosan derivative possessing $-CH_2COOH$ group at its C6 position retains the advantages of chitosan but shows better water solubility and antibacterial activity[40-42]. It is an amphoteric polyelectrolyte and has drawn great attention as a surface coating material for inorganic NPs due to presence of abundant carboxyl and amine groups which may provide stabilization both by physical adsorption and chemical ligation[43,44]. For understanding the physiological properties of drug delivery vehicles, simultaneous tracking of drug delivery vehicle is also necessary.

Optical imaging is one of the easy and simplest methods to track drug delivery vehicle and it also serve the purpose of bio-imaging. Among various optical imaging probes, C-dots have emerged as new advancement in medicine and theranostics due to their exceptional high aqueous solubility,[45] biocompatibility[46], typical optical properties[47], nontoxic precursors as carbon sources, easy surface passivation, strong fluorescence and outstanding photostability[48]. Furthermore, aromatic drugs can be loaded on C-dots through strong $\pi - \pi$ interactions due to graphitic structure of C-dots, hence it has promising application as drug carrier for disease[49].

In present study, we have introduced mesoporous layer of manganese silicate on silica NPs inspired by the previous works to fabricate mesoporous NPs simply by self sacrifice of silica NPs and *in situ* growth of metal silicate layer[24,26-28]. This strategy was not only beneficial in regulating biodegradation but also imparted tumor sensitive responsiveness for controlled drug delivery and mesoporous structure provided high volume for drug loading. CMC coating was facilitated by presence of abundant carboxyl and amino groups which provide better metal chelation sites. CMC coating imparted water dispersibility and biocompatibility as well as itself acted as a source for C-dot precursor. Introduction of C-dots on the surface of manganese silicate NPs provided cellular imaging ability to nanoarchitecture. Cellular imaging was performed on SW480 cell lines. Drug delivery studies, evaluated in physiological pH, acidic pH (6.4 and 5.0) and acidic and reducing environment of glutathione (a common reducing agent present in very high level almost 100-1000 fold in human cancer cells as compared to normal tissues)[50,51], revealed that drug release was more prominent in reducing and acidic environment.

MATERIALS AND METHODS

Materials

Low molecular weight chitosan (Sigma Aldrich), monochloroacetic acid and tetraethylortho silicate (TEOS) were obtained from TCI, India. Ammonia solution (25%), ethanol and manganese acetate were purchased from Merck. NaOH and isopropanol were bought from CDH. All the chemicals were of analytical (AR) grade. Milli Q water was utilized throughout all experiments. Nutrient agar and Nutrient broth used for culturing bacteria were provided by Titan Biotech Ltd., Rajasthan, India. Dulbecco's modified eagles medium (DMEM), Fetal Bovine Serum (FBS), trypsin and anti-anti(antibiotic-antimycotic) were purchased from Gibco Life Technologies, USA. Colon cancer cells (SW480) were received from the national center for cell sciences (NCCS), Pune, India. Human pathogenic bacteria strains Bacillus subtilis (MTCC 121) and

Escherichia coli (MTCC 433) were obtained from IMTECH, Chandigarh, India.

Characterization

Fourier transform infrared (FTIR) spectra of all samples were recorded on KBr pellets on Nicolet 170 SXFT-IR spectrophotometer, operating at 400-4000 cm^{-1} and resolution of 8 cm^{-1}. Double beam spectrophotometer (Shimadzu UV-2450) was used to record UV-visible absorption spectra of all samples using slit width of 2 nm and equipped with quartz cells of 1 cm light path length. Fluorescence properties were assessed by Perkin Elmer LS-45 Fluorescence Spectrometer. Fluorescence spectra were recorded for excitation wavelength of 300-400 nm with 20 nm increment in wavelength. Particle size and polydispersity index (PDI) were determined by dynamic light scattering (DLS) measurement at temperature stabilized to 30±0.1 °C using a Nano Microtrac total solution. The crystallinity of prepared samples were determined by X-ray diffraction (XRD) patterns performed in the range of 5°–80° and 4° min^{-1} scan rate on Rigaku Smart lab diffractometer. Surface area and pore volume was determined on Smart Sorb 92/93 Surface Area Analyser. Live cell imaging experiments were performed on fluorescence inverted microscope (EVOS Microscope, USA) with three filters (GFP, RFP and DAPI). Lyophilizer (S.C. Dey. Co. Kolkata, India) was used for drying polymer samples.

Preparation of SiO_2 NPs

SiO_2 NPs was prepared by well known sol-gel chemistry. Briefly, liq. NH_3 (25%, 2.5mL) was added in a mixture of ethanol (90 mL) and water (13 mL). Subsequently, 2mL TEOS was added to above solution at room temperature with vigorous magnetic stirring. A milky white solution was obtained after some time. The reaction mixture was further subjected to continuous vigorous stirring for 4 h. The resultant product was obtained by centrifugation and several times washing with ethanol. Subsequently it was dried overnight at 60 °C.

Preparation of $MnSiO_3$

0.15 g of SiO_2 was dispersed in 50 mL water assisted by ultrasonication. 7 mmol of manganese acetate was added to the addition dispersion under ultrasonication and sonication was continued for another 1 h. Further, it was transferred to a 50 mL Teflon lined steel autoclaved and placed in a preheated hydrothermal oven maintained at 100 °C for 24 h. Subsequently, obtained solution was centrifuged at 10,000 rpm for 10 min, followed by several times washing.

Preparation of CMC

CMC was synthesized with slight modification in method adopted by Chen and Park[52]. In brief, 2g of chitosan was alkalized in 15 mL saturated NaOH aqueous solution and frozen overnight. Thaw swollen chitosan solution was transferred to 60 mL isopropanol followed by gradual addition of 6 g monochloroacetic acid (dissolved in 2 mL isopropanol) and left for 12 h under gentle magnetic stirring at room temperature. Finally pH was adjusted to 7.0 by addition of HCl. Isopropanol was filtered off and white precipitate obtained was repeatedly washed with ethanol. The solid product was vacuum dried at room temperature. Again, the solid was dispersed in water and unreacted chitosan was removed by centrifugation. Water-soluble portion was lyophilized to obtain pure CMC.

Preparation of CMC@$MnSiO_3$ and CD@CMC@$MnSiO_3$

To obtain CMC coated manganese silicate NPs, the obtained NPs were re-suspended into aqueous solution of CMC (1 mg/mL, 20 mL) under ultrasound treatment for 5 h, and the process was repeated twice for efficient CMC coating. 40 mL of CMC coated $MnSiO_3$ (CMC@$MnSiO_3$) was transferred in a 50 mL Teflon-lined hydrothermal bomb and kept in preheated hydrothermal oven at 160 °C for 6 h. Resultant product was obtained by centrifugation followed by repeated washing and freeze-dried.

Drug loading efficiency

CD@CMC@$MnSiO_3$ (50 mg) were suspended into 90 mL Milli Q containing small amount of CMC (5mg) assisted by ultrasonication, followed by addition of 10 mL curcumin solution (1mgmL^{-1}). Above solution was stirred overnight at room temperature under dark condition. Curcumin loaded CD@CMC@$MnSiO_3$ were collected by centrifugation at 10,000 rpm for

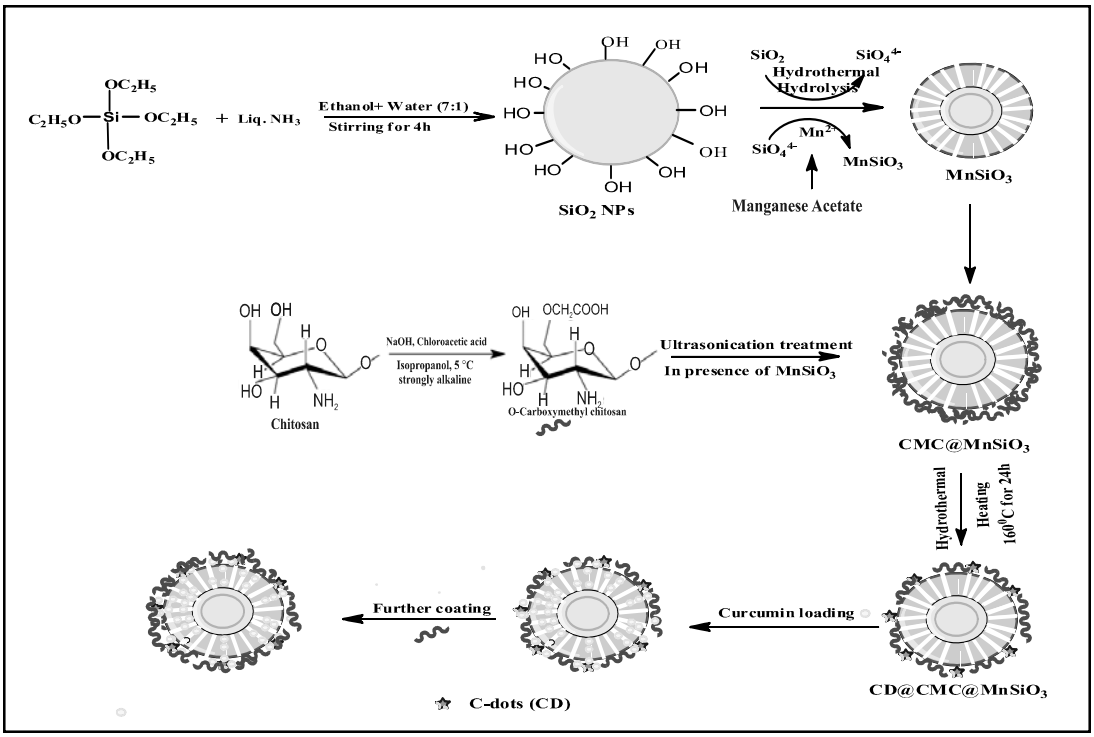

Fig. 1. Schematic illustration of synthesis and drug loading on CD@CMC@$MnSiO_3$ nanoachitecture

20 min and dried at 50 °C in vacuum oven. The effective curcumin loading capacity of CD@CMC@$MnSiO_3$ was determined by measuring the UV-vis absorbance (at 428 nm) of supernatant obtained after centrifugation. Calibration curve of curcumin was plotted by measuring absorbance of curcumin for concentration ranging from 0.1-1 $mgmL^{-1}$ under same condition. Drug entrapment efficiency and loading content was quantified by using following formulas:

$$\text{Drug entrapment efficiency (\%)} = \frac{\textit{Initial amount of drug – free drug}}{\textit{Initial amount of drug}} \times 100$$

$$\text{Drug loading contents (\%)} = \frac{\textit{Amount of drug loaded in carrier}}{\textit{Amount of drug carrier taken}} \times 100$$

Drug Delivery Studies

An important property of drug delivery systems is the controlled release of drugs from the carrier. The pH-controlled release of curcumin by nanoarchitecture CD@CMC@$MnSiO_3$ was investigated in vitro by comparing the release rates at pH 7.4, which mimics the extracellular environment, and at 6.4 and 5.0, since environment of tumor is acidic. Furthermore drug release was also investigated at acidic pH in presence

of reducing environment of glutathione, since glutathione is a common reducing agent within human cancer cells, whose levels in tumors is almost 100 times higher than those in normal tissues[50,51]. In Brief, curcumin-loaded CD@CMC@$MnSiO_3$ (10 mg) were suspended in 5 mL of PBS with different pH values (pH = 7.4, 6.4, 5.4) and PBS of pH 5.0 containing 0.1 mmol glutathione. The suspension was placed into dialysis bags (cut-off molecular weight: 12k Da) and subsequently put into the releasing buffer medium (45 mL)with different pH values (pH = 7.4, 6.4, 5.0). The buffer media was constantly stirred at 100 rpm and 37 °C in a dark place and the release process of drug was determined by taking off 2 mL aliquot of the dissolution at known time intervals followed by replacement with same volume of PBS. Release curcumin was quantified by taking UV–vis absorbance of the curcumin in the dissolution. Cumulative release is expressed as the overall percentage of curcumin released through the dialysis membrane against PBS over entire time by using the following formula: Where, total absorbance means is the absorbance intensity at different period i.e. 2, 4, 6, ...60 h and initial absorbance is the absorbance intensity at 0 h. Cumulative drug release was calculated with the help of calibration curve of curcumin and calculated as follows:

$$Q_n = C_n V_0 + \sum_{i=1}^{n-1} C_i V_i$$

$$R(\%) = \frac{Q_n}{W} \times 100$$

Where, Q_n– Accumulative drug release amount

C_n– concentration of drug in release medium

V_0– Total volume of release medium

V_i– Volume of withdrawn aliquots

C_i– Concentration of drug in release medium at time i

R(%) – Cumulative release percent

W– Total amount of drug in each dialysis bag

Cell Culture and Live cell Imaging

Excellent photoluminescence, aqueous dispersibility, small size (below 200 nm) fostered nanoarchitecture CD@CMC@$MnSiO_3$ as promising imaging probe for cellular imaging. Human colon cancer cells SW480 were employed to evaluate the practical application of CD@CMC@$MnSiO_3$ for live cell imaging. Stock SW 480 cell lines were cultured in DMEM supplemented with 10% FBS, anti-anti and sodium bicarbonate ($2gL^{-1}$) in humidified environment of incubator with 5 % CO_2 and maintained at 37 °C. The cells were passaged every 3-4 days. For cellular imaging experiments, trypsinized cells were seeded in tissue culture plates (24 well plates) at an initial cell density of ~20,000 cells/well and were incubated in CO_2 incubator for 24 h. Subsequently, exhausted media was taken off and cells were gently washed three times with PBS (10 mmol L^{-1} and pH 7.4). Then, cell were treated with 500 µL fresh DMEM containing different concentrations of CD@CMC@$MnSiO_3$ (0.1-0.5 $mgmL^{-1}$) prepared by extensive ultrasonication for 1 h. After overnight incubation for 12 h the cells were further washed with PBS three times and assessed for fluorescence cellular imaging under inverted fluorescence microscope. Fluorescent and bright field images of SW480 cells were obtained under the 20x objective with an exposure time of 5 s.

Antibacterial assessment

The antibacterial assessment of prepared material was performed on both gram positive and gram negative bacteria. For this, *E. Coli* (Gram negative) and *B. Subtilis* (Gram positive) were taken as representative of human pathogenic bacteria. Antibacterial activity was determined through agar disc diffusion method. In brief, nutrient agar (3.5 g in 100 mL water) and nutrient broth (0.65 g in 50 mL water) were prepared and sterilized in autoclave maintained at 15 psi and 121°C for 20 min. Nutrient Broth was used as growing medium for the bacteria. Nutrient agar media was poured in autoclaved petridish and loopful of strains of both pathogen bacterias- *E. Coli* and *B. Subtilis* were streaked on nutrient agar and thus incubated at 37°C for 24 h to cultivate the single colonies. A typical bacteria colony was taken off with the help of an inoculating loop, placed in already sterilized nutrient broth and then

incubated overnight at 37°C for 12 h. Then prepared bacteria medium was dispensed on to agar plate and two wells were bored with the help of sterile cork borer in the centre of agar plates. Finally 1 mL of each sample solution was placed on to agar plate in each well and labeled. Concentration of both CD@CMC@$MnSiO_3$ and $MnSiO_3$ for the test was choosen 100 μgmL^{-1}, $MnSiO_3$ was taken as positive control. This incubation was done for 12 h at 37°C and finally antibacterial efficacy was determined by analyzing zone of inhibition.

RESULTS AND DISCUSSION

Silica NPs (SiO_2) was prepared by Stöber sol-gel method. Mesoporous manganese silicate shell on silica NPs ($MnSiO_3$@SiO_2 but we have used only $MnSiO_3$ for the sake of brevity) was introduced by hydrothermal method under mild condition inspired by previous reports[26-29]but alkaline conditions were avoided. *In situ* silicate growth was formed by consumption of SiO_2 layer. The mechanism behind this process may be first hydrolysis of SiO_2 NPs into silicate anions followed by interaction with manganese ions in the interfacial region, resulting in formation of mesoporous siliacate shell on SiO_2 NPs. CMC coating was successfully introduced on $MnSiO_3$ NPs via metal chelation, since it possess excellent metal chelating property due to presence of abundant hydroxyl, amino and carboxyl groups. Formation of C-dots under hydrothermal condition was facilitated by self carbonization of CMC. The proposed mechanism is well supported by DLS histogram of SiO_2, $MnSiO_3$, CMC@$MnSiO_3$ and CD@CMC@$MnSiO_3$. DLS histogram depicts that synthesized SiO_2 possess size round 120-500nm. The size was significantly reduced after formation of $MnSiO_3$ due to self sacrificing of silica layer. After CMC coating, again increase in hydrodynamic size was observed due to thick CMC layer and hydrogen bonding by –OH, NH_2 and –COOH groups present in CMC. After formation of CDs on CMC@$MnSiO_3$ again decrease in hydrodynamic size was observed along with decrease in PDI. The reason may be due to self aggregation of CMC leading to carbonization. The formation of CDs from various precursors is well documented.CMC precursor undergoes decomposition and form pyranose ring during carbonization[53].

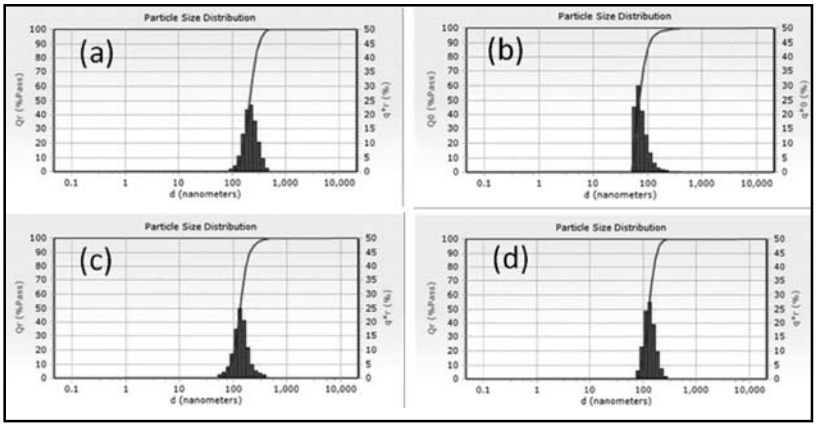

Fig. 2. DLS histrogram of (a) SiO_2, (b) $MnSiO_3$, (c) CMC@$MnSiO_3$ and (d) CD@CMC@$MnSiO_3$

Since, chitosan is a semi-crystalline polymer it shows intense peak around 20° while two small peaks around 9° and 29° are also observed in XRD diffractogram[54-56]. Peak around 20° attributes to (020) plane of orthorhombically interconnected through strong intermolecular hydrogen bonds. After modification of chitosan to CMC, considerable decrease in peak intensities were observed which suggests amorphous nature of CMC, as expected [57]. SiO_2 shows amorphous structure and a broad peak centred around 25° was depicted in X-ray pattern. After hydrothermal treatment, major peaks at 20.1°, 30.4°, 31.8°, 32.9°, 36.8°, 38.2°, 50.8°, 56.4° and 64.5° well matches with the standard α-phase of $MnSiO_3$ (JCPDS No. 12-0181). While other major peaks centred at 15.5°, 40.1°, 42.4°, 49.5° and 52.9° attributes to presence of other phases of manganese silicate. The peaks obtained for manganese silicate is well in accord with, demonstrating successful formation of manganese silicate NPs. After coating of CMC on $MnSiO_3$ NPs, the crystallinity was somewhat reduced, while characteristic peaks of $MnSiO_3$ were still observable. Formation of C-dots resulted in

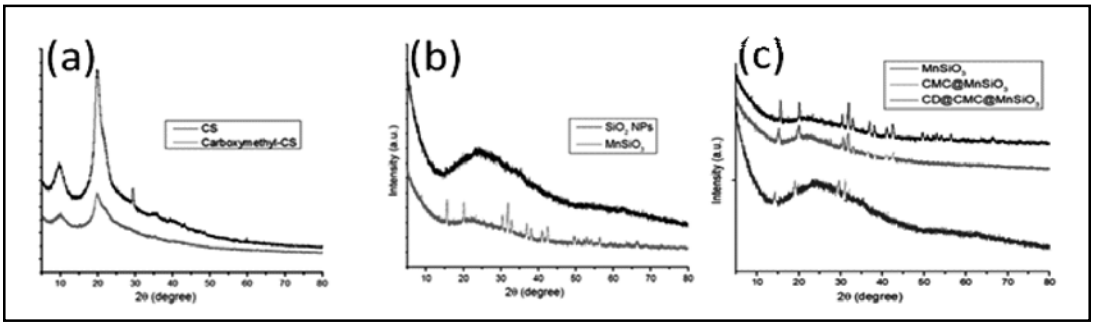

Fig. 3. XRD pattern of (a) CS and CMC, (b) SiO_2 and $MnSiO_3$ NPs (c) CMC@$MnSiO_3$, CMC@$MnSiO_3$ and CD@CMC@$MnSiO_3$

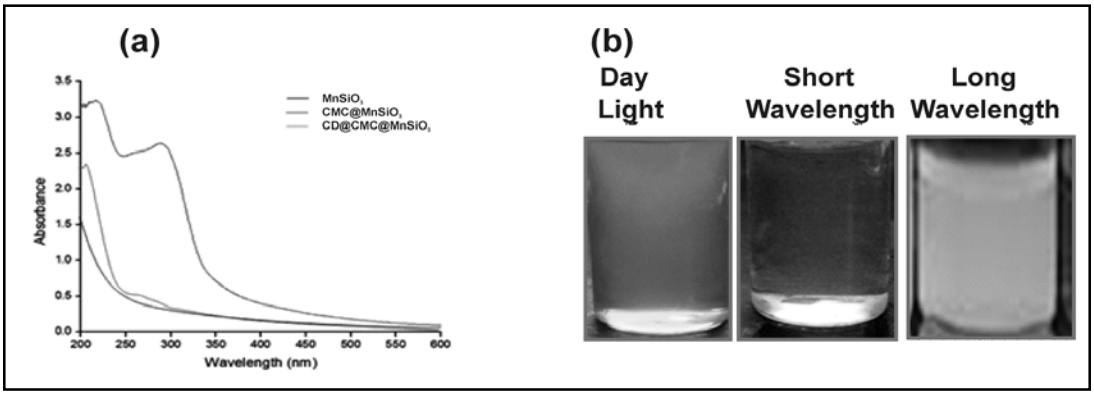

Fig. 4. (a) UV-vis spectra of $MnSiO_3$, CMC@$MnSiO_3$ and CD@CMC@$MnSiO_3$
(b) Photographic images of $MnSiO_3$C-under day light, short wavelength (UV light) and long wavelength

broad peak centred around $2\theta=25^0$ corresponds to many disordered graphitic layers present in C-dots. Surface area and pore volume of $MnSiO_3$ was calculated to be 351.99 m^2/g and 0.3171 cm^3/g respectively. Average pore diameter of $MnSiO_3$ was determined to be 3.6 nm, calculated by using surface area and pore volume values (details have been shown in appendix).

$MnSiO_3$ and CMC@$MnSiO_3$ showed no obvious absorption spectra in 200 nm to 600 nm range, while absorption peaks centered around 220 nm and 290 nm for CD@CMC@$MnSiO_3$ strongly affirming the formation of C-dots on surface of CMC@$MnSiO_3$. The two peaks around 220 nm and 290 nm obtained for $MnSiO_3$ in aqueous medium (0.5 mg/mL) attributes to $\pi - \pi^*$transition (C=C of graphite structure) and $n - \pi^*$ transition(C=N and C=O). This is well consistent with previous reports [58,59 (a,b)].

CD@CMC@$MnSiO_3$ shows excitation wavelength dependent emission spectra with a tail extending towards long wavelength region. Interestingly, it shows three emission bands, a narrow emission band is observed near short wavelength while broad band is obtained towards longer wavelength. CD@CMC@$MnSiO_3$ shows a gradual red shift in emission spectra with increase in excitation wavelength, well coinciding with previous reports [60]. This complex phenomenon occurs due to presence of various emitting centers on surface of C-dots and quantum confinement effect [61]. Maximum intensity was observed at 420 nm for excitation wavelength of 340nm. Beyond 340 nm the PL intensity diminishes gradually.

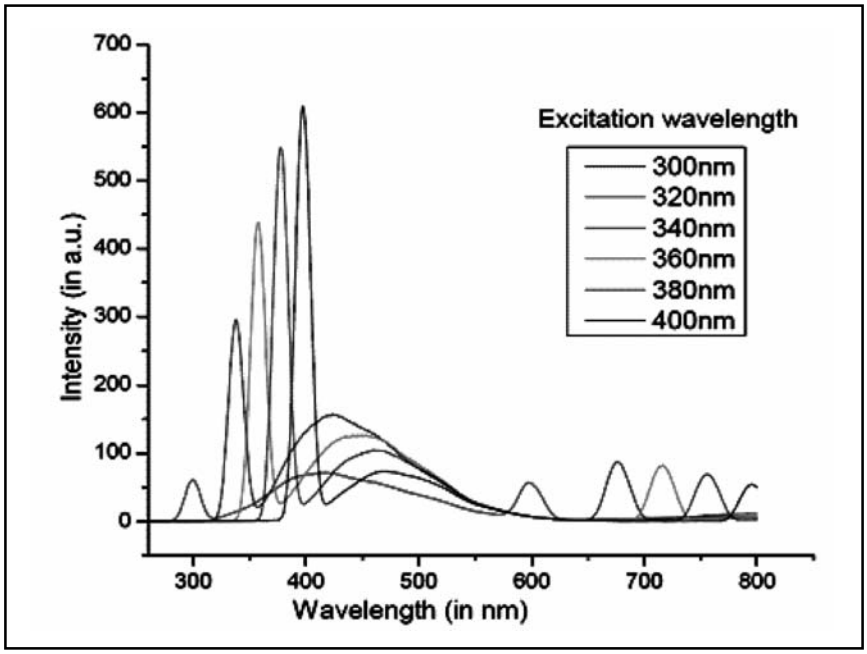

Fig. 5. Photoluminescence spectra of $MnSiO_3$ under different excitation wavelength

FTIR spectra of $MnSiO_3$, CMC, CMC@$MnSiO_3$ and CD@CMC@$MnSiO_3$ are shown in Fig.6. $MnSiO_3$ displays major peaks at 3401.63 cm^{-1}, 1110.26 cm^{-1} , 807.27 cm^{-1} and 473.49 cm^{-1} which may be assigned to O-H/Si-O-H stretching, Si-O-Si stretching, Si-O-C stretching and Mn-O stretching respectively. Several peaks may be depicted in FTIR spectra of CMC which may be assigned as follows: broad peak at 3439.24 cm^{-1} may be assigned to O-H/N-H stretching, 2922.07 cm^{-1} to C-H stretching, 1629.92 cm^{-1} to bending of primary amine groups and 1377.67 cm^{-1} to C-O-C vibrations. A peak centred at 1702.91 cm^{-1} suggests the successful carboxymethylation of chitosan, which is absent in FTIR spectra of CS. A new peak at 470.23 cm^{-1} was clearly discernible in FTIR spectra of CMC@$MnSiO_3$ which confirms the successful coating of CMC on $MnSiO_3$. Slight shift in other peaks were also observed after CMC coating. FTIR spectra of CD@CMC@$MnSiO_3$ was almost similar to that of CMC@$MnSiO_3$ which indicates that functional groups of CMC were still present on the surface after hydrothermal treatment.

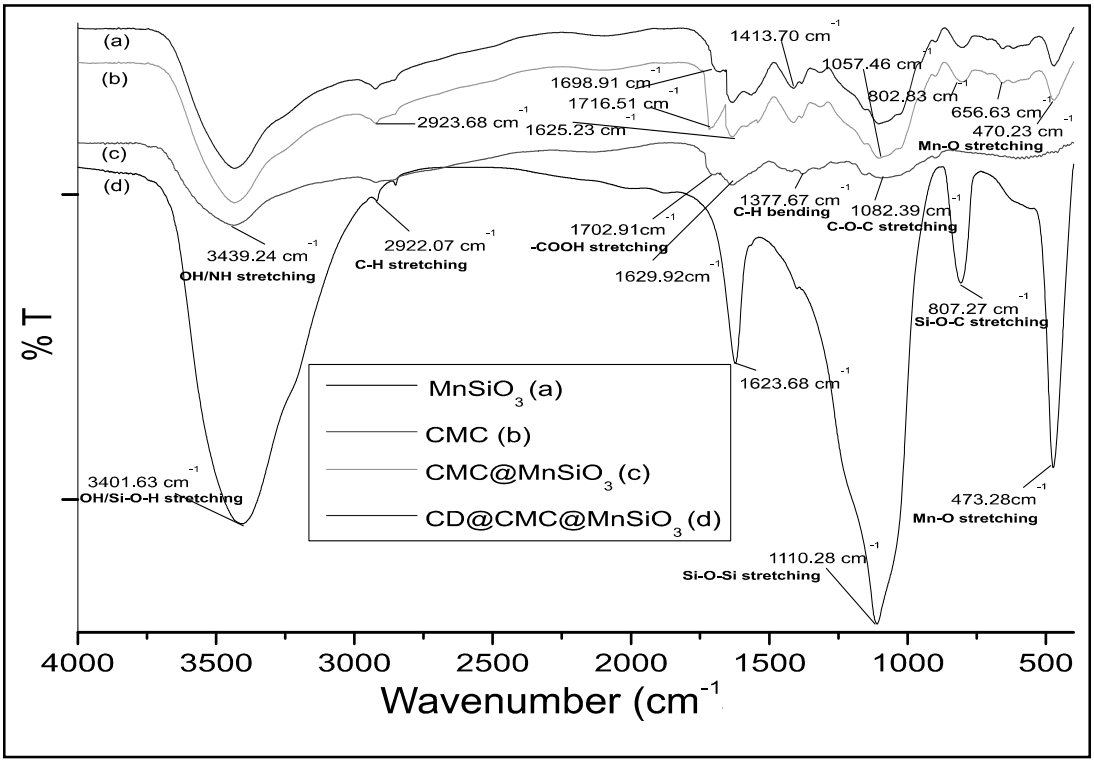

Fig. 6. FTIR spectrum of $MnSiO_3$, CMC, CMC@$MnSiO_3$ and CD@CMC@$MnSiO_3$

Drug loading efficiency and drug loading content

Drug loading content and drug entrapment efficiency of curcumin in CD@CMC@$MnSiO_3$ were found to be 15.6% and 78.1%, respectively. High loading content as high as 15.6 might suggest mesoporous structure of CD@CMC@$MnSiO_3$. The loading of curcumin into the CD@CMC@$MnSiO_3$ is due to the physisorption of curcumin through van der Waals interaction, supramolecular π-π stacking and hydrophobic attraction to C-dots present on surface of CD@CMC@$MnSiO_3$.

Drug release study

Drug release performance was studied under different pH conditions (7.4, 6.4 and 5.0) and in presence of glutathione also at 37 °C. The drug release profile demonstrated that the release rate was more favorably triggered by decrease in pH of release medium. It was found that only about 4% of curcumin was released at pH 7.4, whereas nearly 38% and 70% was released at pH 6.4 and pH 5.0 respectively in the same time duration (Fig. 7). This pH triggered facile drug release might be attributed to swelling of CMC due to protonation of amino groups in acidic environment, increased solubility of curcumin under acidic condition. Another reason may be rupture of pH sensitive Mn-O bonds and exchange of manganese ions in manganese silicate with hydrogen protons under acidic condition. Drug release study showed that curcumin release was much more prominent in presence of reductive environment of glutathione and acidic environment. However, in presence of glutathione the drug released was found to be 89.3%. This expedite drug release might be associated with the degradation of manganese silicate due to presence of some manganese ions in higher oxidation states in presence of glutathione. So, the best result was obtained for acidic and reducing environment prevalent to tumor environment. Thus, the release pattern of drug indicates a dual response drug release assisted by key roles of both pH-responsive CMC and Mn-O bond as well as glutathione responsive manganese release. This release pattern is very

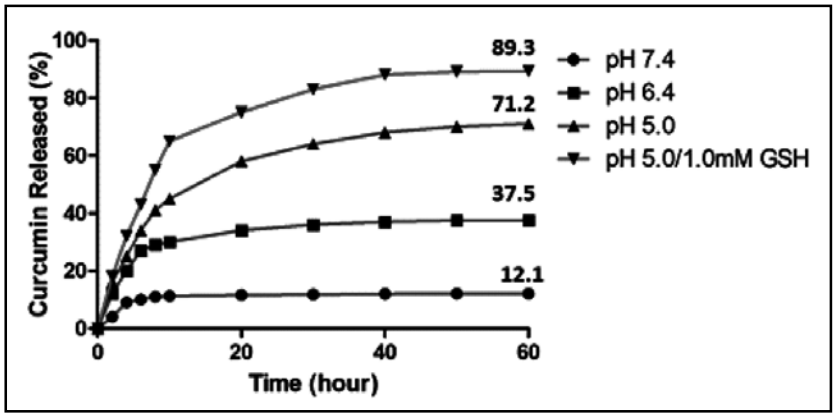

Fig. 7. Drug release pattern of curcumin-loaded CD@CMC-$MnSiO_3$ in PBS of different pH values (7.4, 6.4 and 5.0) and in the presence of 1 mM glutathione in PBS buffer at pH = 5.0

promising to reduce side effects of chemotherapy to normal tissues and increasing efficacy of chemotherapy after being endocytosized in cancer cells.

Cell culture and Live cell Imaging

We introduced CD@CMC@$MnSiO_3$ into target cells SW 480 for *in vitro* bioimaging using fluorescence microscopy. Fig.8(a) shows the bright-field image and Fig. 8 (b) and (c) shows fluorescent images of SW480 cells incubated with CD@CMC@$MnSiO_3$, observed under UV light excitation. Fluorescence imaging results show that, after 12 h incubation with the target cells SW 480, green photoluminescence could be observed in the areas of the cell membrane and cytoplasmic area of the cells. The results demonstrated that CD@CMC@$MnSiO_3$ was easily uptaken by cells but not able to penetrate the cell nuclei. Hence CD@CMC@$MnSiO_3$were successfully uptaken by SW 480 cells without affecting cell functioning. Furthermore, no damage and morphological changes were observed in the cells, that confirms the low cytotoxicity of the CD@CMC@$MnSiO_3$. These results reveal that the obtained our prepared material have promising applications in cellular imaging as well as tracking of drug vehicle via fluorescence microscopy, which is important for study of kinetics and fate of drug.

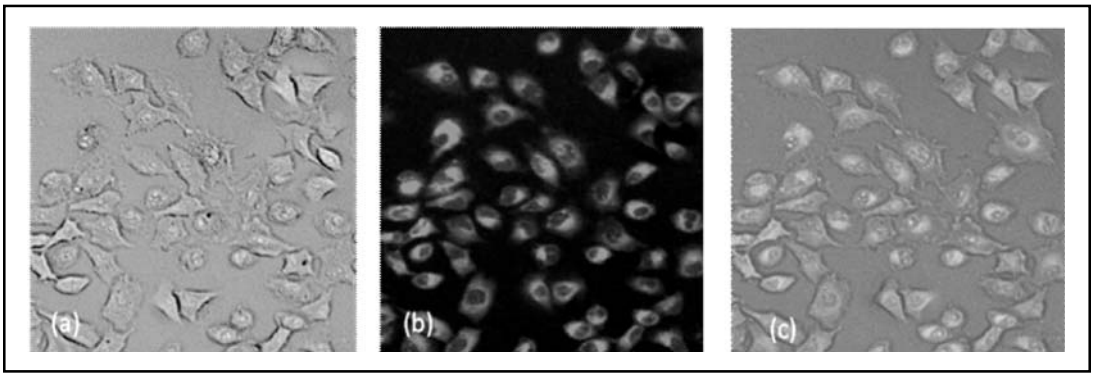

Fig. 8. Fluorescence microscopy images of SW480 cells labelled with CD@CMC@$MnSiO_3$: (a) Bright field image; (b) green field (c) merge images of (a) and (b)

Antibacterial assessment

Since, antibacterial activity is the foremost desired property for preventing drug from enzymatic degradation. Our prepared material displayed excellent antibacterial property against both gram positive and gram negative bacteria, which is clear from distinct zone of inhibition in Fig. 9. The antibacterial activity analysis shown in Table 1 depicts the zone of inhibition (in mm) of various samples. All samples showed higher antibacterial property against gram negative bacteria. The reason behind excellent activity might be due to interaction of positively charged amino groups in CMC with the negatively charged phosphorous and sulfur compounds present in proteins and nucleic acid of bacteria, this result in structural changes and deformation of cell

wall and cell membrane and ultimately leading to cell death. Antibacterial activity found in $MnSiO_3$ may be due to its small size which can easily diffuse through bacterial and affecting the transport of essential nutrients through membrane, hence affecting functioning of physiological activity of bacteria.

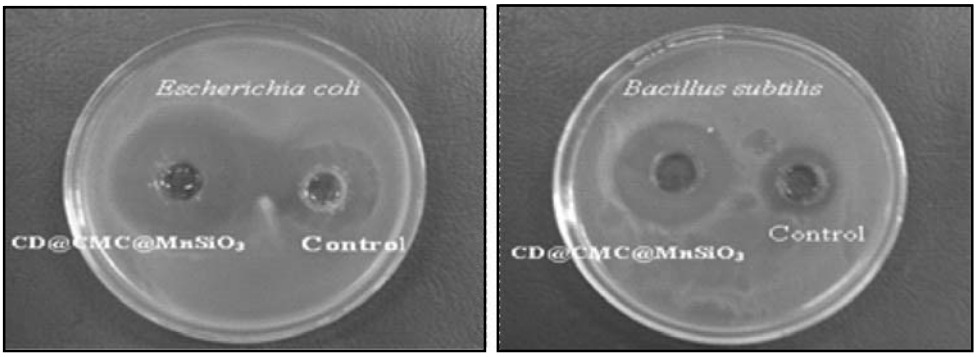

Fig. 9. Zone of inhibition of $MnSiO_3$ and CD@CMC@$MnSiO_3$ against two different bacterial strains

TABLE 1. Zone of inhibition of bacteria

Bacteria	Inhibition zone against Bacteria (in mm)	
	Control ($MnSiO_3$)	CD@CMC@$MnSiO_3$
E. Coli	25 ± 2	42 ± 2
B. Subtilis	23 ± 2	38 ± 2

CONCLUSION

In present study, we have prepared a C-dot integrated metal ion doped stimuli nanocarrier by using a facile and easy method. Prepared materials were investigated by different characterization techniques. Antibacterial activity, drug release studies, cell imaging experiments were also carried out. Results revealed that prepared nanocarrier displayed stimuli responsive (tumor environment) release behavior and excellent antibacterial property against both gram positive and gram negative pathogenic bacteria. Tumor environment responsive manganese release may also be applied in manganese enhanced magnetic resonance imaging with very low signal background in normal tissues. In this way, we have presented a facile strategy to synthesize nanoarchitecture with multifunctional applications.

Acknowledgement

One of the authors, P.B. is grateful to Director Prof. Rajeev Tripathi, MNNIT, Allahabad, India, for providing the stipend and infrastructure for characterization (Centre for interdisciplinary research, CIR). We would also like to thank Material Research Centre (MRC), MNIT, Jaipur for FTIR analysis.

REFERENCES

1. G. Chen, I. Roy, C. Yang and P. N. Prasad, *Chem. Rev.* **116 (**2016) 2826.
2. Y. Chen, C. Tan, H. Zhang and L. Wang, *Chem. Soc. Rev.* **44** (2015) 2681.
3. E. Terreno, F. Uggeri and S. Aime, *J. Controlled Release,* **161** (2012) 328.
4. K. Yang, L. Z. Feng, X. Z. Shi and Z. Liu, *Chem. Soc. Rev.* **42** (2013) 530.
5. D. Peer, J.M. Karp, S. Hong, O.C. FaroKHzad, R. Margalit, R. Langer, *Nature Nanotech.* **2** (2007) 751.
6. S. Mura, J. Nicolas and P. Couvreur, *Nat. Mater.* **12** (2013) 991.
7. J.M. Rosenholm, V. Mamaeva, C. Sahlgren and M. Linden, *Nanomedicine (Lond)* **7** (2012) 111.
8. Z. Li, J.C. Barnes, A. Bosoy and J.F. Stoddart,*Chem. Soc. Rev.* **41** (2012) 2590.
9. C.E. Fowler, D. Khushalani and S. Mann, *Chem. Commun.* **279** (2001) 2028.
10. Y. Zhu, J. Shi, W. Shen, X. Dong, J. Feng, M. Ruan, Y. Li, *Angewandte Chemie* **117** (2005) 5213.
11. M. Ma, H. Chen, Y. Chen, X. Wang, F. Chen, X. Cui, J. Shi, *Biomaterials,* **33** (2012) 989.
12. L. Pan, Q. He, J. Liu, Y. Chen, M. Ma, L. Zhang, J. Shi, *J. Am. Chem. Soc.* **134** (2012) 5722.
13. J. Liu, W. Bu, L. Pan and J. Shi, *Angew. Chem.-Int. Edit.* **52** (2013) 4375.
14. Q. He, J. Shi, F. Chen, M. Zhu and L. Zhang,*Biomaterials,* **31** (2010) 3335.
15. Q.J. He and J.L. Shi, *J. Mater. Chem.* **21** (2011) 5845.
16. Y. Chen, H. Chen, L. Guo, Q. He, F. Chen, J. Zhou, J. Feng, J. Shi, *ACS Nano,* **4** (2010) 529.
17. I.I. Slowing, J.L. Vivero-Escoto, C.W. Wu and V.S. Lin, *Adv. Drug Deliv. Rev.* **60** (2008) 1278.
18. J. Lu,M. Liong, Z. Li, J.I. Zink and F. Tamanoi, *Small,* **6**(2010) 1794.
19. Y. Zhao, T. Ji, H. Wang, S. Li, Y. Zhao and G. Nie, *J. Controlled Release,* **177** (2014)11.
20. L. Wang and C. Li,*J. Mater. Chem.* **21** (2011)15862.
21. C. H. Tung, J. Qi, L. Hu, M. S. Han and Y. Kim, *Theranostics,* **5** (2015)1166.
22. L. Dong, S. Xia, K. Wu, Z. Huang, H. Chen, J. Chen and J. Zhang, *Biomaterials,* **31** (2010) 6309.
23. A. Zhu, K. Miao, Y. Deng, H. Ke, H. He, T. Yang, M. Guo, Y. Li, Z. Guo, Y. Wang, X. Yang, Y. Zhao and H. Chen, *ACS Nano,* **9** (2015) 7874.
24. Yu L, Chen Y, Wu M., Cai X., et al, *J. Am. Chem. Soc.* **138** (2016) 9881.
25. J. Li, Z. Zhao, J. Feng, Gao J and Z. Chen, *Nanotechnology,* **24** (2013) 455102.
26. Q. Fang, S. Xuan, W. Jiang and X. Gong, *Adv. Funct. Mater.* **21** (2011)1902.
27. J. Yang, M. Zhang, Y. Zhang, L. Dinget al, 10.1016/j.jallcom.2017.06.038.
28. Y. Ling, Q. Gao, C.F. Ma, Y.S. Gong et al, *RSC Adv,* **6** (2016) 23360.
29. F. Zhang, Y. An, W. Zhai, X. Gao et al, *Mater. Res. Bull.* **70** (2015) 573.
30. E.K. Larsen, T. Nielsen, T. Wittenborn and H. Birkedal, *ACS Nano,* **3**(2009)1947.
31. C.M. Lee, H.W. Jeong, E.M. Kim, S.J. Cheong et al, *Macromol. Res.* **17** (2009) 133.
32. H.Y. Lee, N.H. Lim, J.A. Seo, S.H. Yuk et al, *J. Biomed. Mater. Res., Part B* **79** (2006) 142.
33. Y.Y. Liang and L.M. Zhang, *Biomacromolecules,* **8** (2007) 1480.
34. C.L. Lin, C.F. Lee and W.Y. Chiu, *J. Colloid Interface Sci.* **291** (2005) 411.
35. P.K Dutta, Chitin and chitosan for regenerative medicine, Springer, (2016).

36. D. Archana, J. Dutta and P.K. Dutta,*Int. J. Biol. Macromol.* **57** (2013) 193.

37. D. Archana, B.K. Singh, J. Dutta, P.K. Dutta, *Carbohyd. Polym.* **95** (2013) 530.

38. P.K. Dutta, R. Kumari and J. Dutta, Chitosan: A promising biomaterial for tissue engineering scaffolds, *Chitosan for Biomaterials II,* 45 (2011).

39. J.H. Park, G. Saravana kumar, K. Kim and I.C. Kwon, *Adv. Drug Deliver. Rev.* **62** (2010) 28.

40. X.F. Liang, H.J. Wang, H. Luo, H. Tianet al, *Langmuir,* **24** (2008) 7147.

41. T.Y. Liu, S.Y. Chen, Y.L. Lin and D.M. Liu, *Langmuir,* **22** (2006) 740.

42. M. Prabaharan and S. Gong,*Carbohydr.Polym.* **73** (2008) 117.

43. A.P. Zhu, M.B. Chan-Park, S. Dai and L. Li, *Colloids Surf. B,* **43** (2005) 143.

44. A. Zhu, L. Yuan and Y. Lu, *Colloid Polym. Sci.* **285** (2007) 1535.

45. X. Xu, R. Ray, Y. Gu, H.J. Plohn et al, *J. Am. Chem. Soc.* **126** (2004) 12736.

46. P. Bhartiya, A. Singh, H. Kumar, T. Jain et al, *J. Indian Chem. Soc.* **93** (2016) 1.

47. J.H. Shen, Y.H. Zhu, X.L. Yang and C.Z. Li, *Chem. Commun.* **48** (2012) 3686.

48. S.Y. Lim, W. Shen and Z. Gao,*Chem. Soc. Rev.* **44** (2015) 362.

49. S. Rai, B.K. Singh, P. Bhartiya, A. Singh, H. Kumar, P.K. Dutta and G.K. Mehrotra, *J. Lumin.* **190** (2017) 492.

50. S.H. CraytonandA. Tsourkas, *ACS Nano,* **5** (2011) 9592.

51. M.H. Lee, Z. Yang, C.W. Lim, Y.H. Lee et al, *Chem. Rev.* **113** (2013)5071.

52. X.G. Chen and H.J. Park, *Carbohydr. Polym.* **53** (2003) 355.

53. X. Liu, J. Pang, F. Xu and X. Zhang, *Sci. Rep.,* **6** (2016) 31100.

54. W. Li-xia, W.Zi-wei, W. Guo-song, L. Xiao-don get al, *Polym. Adv. Technol.* **21** (2010)244.

55. M. Jaworska, K. Sakurai, P. Gaudonand E. Guibal, *Polym. Int.* **52** (2003)198.

56. T. Baran and T. Mentes, *Int. J. Biol. Macromol.* **79** (2015)542.

57. L. Upadhyaya, J. Singh, V. Agarwal and R.P. Tewari, *J. Control. Release,* **186** (2014) 54.

58. X.F. Jia, J. Li and E.K. Wang, *Nanoscale,* **4** (2012) 5572.

59. (a) A. Kumar, A.R. Chowdhuri, D. Laha, S. Chandra, P. Karmakar and S.K. Sahu*, RSC Adv*. 6 (2016) 58979.

(b) P.K. Dutta, T. Ghosh, H. Kumar, T. Jain and Y. Singh, *Asian Chitin J.*, 11(1) (2015) 1.

60. J. Jiang, Y. He, S.Y. Li and H. Cui,*Chem. Commun.* **48** (2012) 9634.

61. Q. Li, T.Y. Ohulchanskyy, R.L. Liu, K. Koynov, D.Q. Wu, A. Best, R. Kumar, A. Bonoiu and P.N. Prasad, *J. Phys. Chem. C,* **114** (2010) 12062.

Received: 15-01-2018

Accepted: 31-01-2018

APPENDIX

Both suface area and pore volume of MnSiO3 measured by BET Surface Area Analyser (Model Smart Sorb 92/93). It is based on dynamic BET principle. The instrument uses a high sensitive thermal conductivity detector to measure the adsorption/desorption signals of nitrogen gas over degassed/ regenrated sample. Surface area and pore volume is automaticallly calculated by the software. We get a graph for thermal conductivity versus time, but the axis in graph we obtains b this instrument isnot defined. So, we had not provided the data for it. Data obtained for surface are and pore volume have been defined. So, we had not provided the data for it. Data obtained for surfacearea and pore volume have been provided below. Surface area and pore volume determined by this instument was found to be 351.99 m2/g and 0.3171 cm3/g respectively. Average pore diameter was also calculated by using following formula:

$$\text{Average pore diameter } (A^0) = 40000 \quad \frac{\text{Total Pore Volume } (\frac{cc}{gm})}{\text{Surface Area } (\text{sq.}\frac{m}{gm})}$$

It was found to be 3.6 nm.

MNNIT

Surface Area Analyser **From Smart Instruments Co. Pvt. Ltd.**	**Model Smart Sorb 92/93** **webSite: www.smartinstrument.com**
Run Time 03:08 pm	Date : June 23, 2017
% of N2:29.94 Sample Name : **MnSiO3** Wt of Tube (gms) : 24828 Sample Wt. (gms) : 0281 Sample Loss : .0% Regeneration Temp. (deg.C) : 200 Time for regeneration (min) : 60	Room temp. in Deg. C:33 Wt of Tube+Sample (gms) : 24.1109 Sample Wt after Reg. (gms) : .0281
Desorption count : 29817.4 Injection count : 8252.731 Injected volume (cc) : 1	

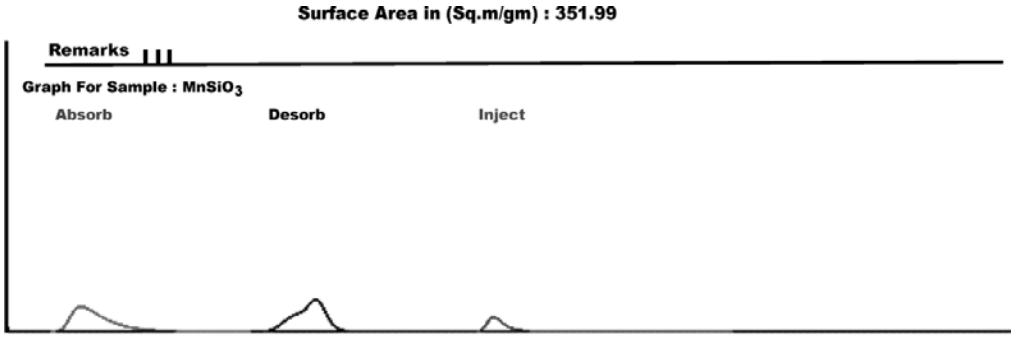

MNNIT

Pore Volume Analyser **From Smart Instruments Co. Pvt. Ltd.**	**Model Smart Sorb 92/93** **webSite: www.smartinstrument.com**
Run Time 03:10 pm	Date : June 12, 2017
% of N2:94.92 Sample Name : **MnSiO3** Wt of Tube (gms) : .24.3249 Sample Loss : .0655 Sample Loss : .0% Regeneration Temp. (deg.C) : 200 Time for regeneration (min) : 90	Room temp. in Deg. C:24 Wt of Tube+Sample (gms) : 24.3904 Sample Wt after Reg. (gms) : .0655
Desorption count : 4616.4 Injection count : 3550.4 Injected volume (cc) : 2.5	

Pore Volume in (cc/gm) : 0.3171